Performance limitations of NbN SIS junctions with Al striplines at 600 - 850 GHz

P. Dieleman, T.M. Klapwijk, H. van de Stadt†,
University of Groningen, Department of Applied Physics and Materials Science Center (MSC) Nijenborgh 4.13, 9747 AG Groningen, The Netherlands.
† Space Research Organisation of the Netherlands, Landleven 12, 9747 AD Groningen, The Netherlands.

M. Schicke, B. Plathner, and K.H. Gundlach
Institut de Radio Astronomie Millimetrique, 300 rue de la Piscine, Saint Martin d'Hères, France.

Abstract

We study the behavior of NbN SIS junctions as radiation detectors with emphasis on the shotnoise generated at voltages below the gap voltage. The intrinsically large subgap current of NbN junctions is carried by pinholes with a conduction attributed to multiple Andreev reflection, leading to transported charges $q >> e$. Using this charge enhancement mechanism we explain the junction shotnoise characteristics in the unpumped case as well as in the pumped case. The measured mixer noise temperature in the pumped case is more than twice that calculated with standard Tucker theory. Measured double side band noise temperatures are 1450 K and 3300 K at 600 and 850 GHz respectively. Main limitations to the receiver sensitivity are the loss in the aluminum circuit and the subgap current induced shotnoise.

1 Introduction

Heterodyne mixers consisting of niobium Superconductor-Insulator-Superconductor (SIS) tunnel junctions are sensitive receivers for radio astronomy in the millimeter and submillimeter wavelength range. There is an increasing demand for these devices at frequencies beyond 700 GHz, which is the frequency limit dictated by the energy gap of Nb. Impedance matching circuits of normal metals are used with a relatively low absorption loss[1, 2]. This allows extension of the upper frequency limit to about 1100 GHz, close to twice the gap frequency of Nb. For detection at higher frequencies a superconductor with a larger energy gap is needed. The most obvious candidate is NbN, with a practical energy gap of 4.8 meV corresponding to a frequency limit of 2 THz. A major drawback of NbN junctions is that the current technology for making high current density junctions leads to an intrinsically large subgap (leakage) current due to pinholes in the barrier. In spite of this, recent results at low frequencies with NbN junctions and (partly) Nb striplines are promising[3, 4] as are the results presented in this paper. To identify room for improvement we investigate the limitations to the sensitivity of NbN SIS mixers with emphasis on the use at THz frequencies. At these frequencies impedance matching circuits made of normal metals provide lower losses than structures made of Nb or NbN[5]. The losses in normal metals are appreciable but well understood and unavoidable[2, 5, 6]. Therefore in this article we will focus on the behavior of the NbN junction itself.
The device characteristics are described in part 2, in part 3 the current-voltage and shotnoise characteristics are presented and modeled. Part 4 compares our measured heterodyne mixing results with the values obtained from the model derived in part 3. Part 5 summarizes the outcome and discusses the expected behavior at supra-THz frequencies.

2 Junction characteristics and measurement setup

The NbN junctions used are fabricated by sputtering on unheated 200 μm thick fused quartz substrates. The NbN films are deposited by reactive RF-magnetron sputtering in an argon and nitrogen atmosphere. The barrier is formed by depositing MgO intermittently on a rotating substrate holder. The junction is patterned by reactive ion etching with CF_4 gas. The MgO layer is etched with a phosphoric acid. We present measurements on two junctions, labeled A and B with resonance frequencies 600 and 850 GHz respectively. The junctions have areas of 0.8 μm^2 and normal resistances R_N of 30 Ω (A) and 50 Ω (B) corresponding to a current density of 15 and 9 kA/cm^2. An I,V curve measured at 4.5 K is shown in Fig. 1a. The subgap-to normal resistance ratio, $R_{(3mV)}/R_N$ is 4.5 and is not improved by lowering the operating temperature. The impedance matching structure is a two junction tuning circuit[7]; two junctions separated by a piece of stripline with length l which serves to transform the capacitive part of the impedance of one junction into an inductive reactance which tunes out the capacitance of the other. A second stripline section of length L matches the resulting real resistance to the antenna impedance, taken to be

50 Ω. The width of both striplines is 4 μm. The striplines and antenna consist of sputtered Al layers with a residual resistance ratio defined as $R_{(300K)}/R_{(5K)}$ of about 3. Details of a similar process are described in [8]. The substrate is polished down to 40 – 50 μm thickness and mounted in a mixer block scaled from a 345 GHz mixer[9]. The mixer is cooled to about 4.5 K. A contacting backshort is used as an adjustable mechanical tuning element. A Mylar beamsplitter of 15 μm thickness is used to inject the local oscillator signal at 600 and 680 GHz, a 56 μm thick beamsplitter is used at 850 GHz. The vacuum window consists of 105 μm thick Mylar and a 110 μm black polyethylene sheet at 77 K functions as IR heat filter. The junctions are connected via an integrated low-pass RF filter and a circulator with 0.5 dB loss to the IF amplifier chain with a noise temperature of 3 K and 80 dB gain at 1.5 GHz with 85 MHz bandwidth.

3 Shot noise measurements and modeling

In Fig. 1a the I,V curve and differential resistance are plotted. Clearly the subgap current is much larger than expected from simple tunneling theory[10]. This can be due to *a)* an energy gap spread over the junction area because of inhomogeneous materials quality , *b)* barrier edge effects, *c)* pinhole defects in the barrier. The first can be excluded since this leads to a gap smearing which is indeed observed, but small, ΔVgap < 0.5 mV. Barrier edge damage can be excluded since large area junctions exhibit the same I,V characteristics as smaller ones where the edge effects should be more dominant, if present. Therefore we conclude that the current transport is through pinholes, small defects in the deposited MgO. The observation of subgap harmonic structures in Fig. 1a supports this conclusion, since these occur only in transparent channels. Together with the independence of the I,V curve on temperature they hint at the transport mechanism in these pinholes causing the excess subgap current, multiple Andreev reflection (MAR)[11, 12].

An electron approaching a superconductor can either reflect normally at the interface or take an electron from the Fermi sea to tunnel jointly into the superconductor to form a Cooper pair (Andreev reflection). The charge effectively transported is 2e. The missing electron (a hole) has opposite phase and momentum and will therefore move away from the interface. If the normal conductor is sandwiched between two superconductors the hole will again have a probability for Andreev reflection at the opposite interface. Since the energy of the Andreev reflected particle is exactly as far above the Fermi level as the original particle was below, the back and forth movement can go on until the electron or hole has gained enough energy to tunnel into one of the superconductors at an energy larger than the energy gap. With each Andreev reflection event a Cooper pair is created or destroyed, and a charge 2e is transferred from the normal regime to the superconductor or vice versa. The average total charge q transported after each tunneling event depends on the Andreev reflection probability and therefore on the transmission of the pinhole. The maximum charge in the limit of high pinhole transmission is calculated following KBT[11]. In this limit an electron coming from the normal region is either Andreev reflected or tunnels into the

superconductor. The total current flowing from the left superconductor (at voltage V) to the right superconductor (at zero voltage) is given by the difference of[11]

$$I_{\rm LR} = \frac{1}{eR_N} \int_{-\infty}^{\infty} dE f_0(E-eV)[1-A(E-eV)][1+A(E)+A(E)A(E+eV)+\cdots] \quad (1)$$

and

$$I_{\rm RL} = \frac{1}{eR_N} \int_{-\infty}^{\infty} dE f_0(E)[1-A(E)][1+A(E-eV)+A(E-eV)A(E-2eV)+\cdots] \quad (2)$$

where $f_0(E)$ is the Fermi distribution, $A(E)$ is the Andreev reflection probability. The first term $[1-A]$ denotes the fraction of available electrons in the superconductor which is transmitted into the normal region. The last term $[1+\cdots]$ gives the proper charge transferred, 1 if no Andreev reflections take place, 2 for one Andreev reflection, and so on. At every voltage the currents I_n $(n = 1, 2, \ldots)$ carried by n-electron processes are calculated by splitting up Eqs. 1 and 2 into the n-electron parts. For example I_2 is given by

$$\begin{aligned} I_2 \;=\; \frac{2}{eR_N} \int_{-\infty}^{\infty} dE(\; & f_0(E-eV)[1-A(E-eV)]A(E)[1-A(E+eV)] - \\ & f_0(E)[1-A(E)]A(E-eV)[1-A(E-2eV)]\;) \end{aligned} \quad (3)$$

The factor 2 comes in because 2e is taken across the normal region. The sum of the properly weighted currents nI_n divided by the total current gives the average charge multiple q/e carried. The resulting charge-voltage curve is shown in the inset of Fig. 1b. The charge is calculated over a small voltage range since the calcuation becomes increasingly time consuming at lower voltages. For this reason a much simpler approach is tried to estimate the average charge. The charge is calculated by taking unity Andreev reflection probability for electrons arriving at energies below the gap energy and zero probability for electrons with higher energies, thereby neglecting higher order terms. The resulting average charge is then simply $m \cdot e$ at voltages Vgap$/(m+1)$, lower than the values obtained using the full energy dependence of the Andreev reflection probability. Since in our case a pinhole is considered to have a short length, the total time of an Andreev reflection sequence is short. With this assumption the charge is considered to tunnel simultaneously. Therefore the calculated charge can be used in the standard low-frequency shotnoise equation[13] :

$$P_{\rm shot} = \frac{1}{4}\,(2qIB \coth \frac{qV}{2k_BT} R_{\rm dyn}) \quad (4)$$

This equation yields good correspondence between the current-voltage and shotnoise characteristics of Nb devices[14]. Fig. 1b shows the shotnoise measured with the IF chain described in section 2 together with the curve calculated using Eq. 4. The best fit was obtained using the solid curve in the inset of Fig. 1b, which is the charge calculated neglecting Andreev reflection above the gap (the dotted curve in the inset), multiplied by a factor 1.1. This input charge is lower than the charge calculated following [11] indicating that the pinhole transmission is lower than 1 since this would result in

a lower Andreev reflection probability as used in the approximation. Clearly the IF output curve calculated using the effective charge concept follows the measured result very well. *Hence the shotnoise of a high current density NbN junction is intrinsically more than doubled!* By high current density we mean 10 kA/cm^2 or more, resulting in a $R_{(3mV)}/R_N$ of 10 or smaller with state of the art technology[15, 16]. Similar shotnoise behavior in NbN junctions was previously observed but not understood[17]. Our results agree with a theoretical prediction which was not yet observed that a single normal metal / superconductor structure can produce a shotnoise up to twice that of a structure consisting of two normal metals due to the 2e charge transfer via Andreev reflection[18].

4 Receiver noise measurements

To investigate the effect of the shot noise behavior of the junction on the mixing properties heterodyne measurements are performed at 600 and 850 GHz using standard hot/cold loads. For each frequency the bias voltage, backshort position and local oscillator power is adjusted to give optimum performance. Fig. 2b shows the IF output power at 600 GHz versus bias voltage for input powers corresponding to 77 K and 293 K. Y-factors and corrected receiver noise temperatures are listed in Table 1. Measured loss values of optical components are listed in Table 2. The stripline loss is derived from the measured receiver gain. The calculated stripline loss is close to the measured value, if the aluminum conductivity derived from the series resistance value is taken into account instead of the independently measured Al conductivity. This lowers the residual resistance ratio to about 3. From wideband FTS measurements it was concluded that the resonance frequency is lower than anticipated. This may indicate a specific capacitance that is larger than the 135 fF/μm^2 which we expect for the current densities found[16]. The effective coupling is also not optimal since the design assumed 18 Ω junctions with sizes of 1 μm^2.

Table 1: Measured receiver noise and gain values

Junction	Frequency (GHz)	Y- factor (dB)	T_{REC} (K)
A	600	0.55	1450
A	680	0.45	1700
B	850	0.15	3300

Table 2: Loss in dB of RF components

Junction	Beamsplitter	Window	Heat Filter	Lens + Horn	Stripline
A (600 GHz)	0.32	0.81	0.81	0.22	7.5
B (850 GHz)	2.9	0.13	0.18	0.22	12

The consequence for the mixer noise temperature is that the same voltage dependent q value has to be applied in the calculation of the current correlation matrix H_{ij}

of the Tucker theory[19]. The resulting mixer noise temperatures are listed in Table 3. Since the effective charge q at the optimum bias voltage is about 2.5, the mixer noise temperatures are increased by approximately the same value. The calculated IF output powers are compared with the measured values in Fig. 2b. In the voltage region of the first photon step, the measured and calculated values agree reasonably well, indicating the validity of the method.

Table 3: Measured and calculated mixer noise T_M and loss L_M. The mixer noise values in column *calc* is calculated using $q = e$, the values labeled *corr* are calculated using the full expression for q.

	T_M (K)			L_M (dB)	
Junction	meas	calc	corr	meas	calc
A (600 GHz)	243	80	198	9.1	9.1
B (850 GHz)	204	77	168	8.1	7.8

5 Conclusions

Sensitive THz radiation detection requires small area, high current density SIS junctions. However, the current NbN/MgO/NbN technology is not matured sufficiently to obtain thin pinhole-free tunnel barriers. Whether it will be possible to further improve the technology to produce MgO barriers with less defects remains to be seen. The presence of pinholes results in a large subgap current with intrinsically large shot noise power due to multiple Andreev reflection. Because of this effect it is unlikely that NbN SIS junctions will outperform Nb junctions below 1100 GHz. To illustrate this: The only difference between NbN junctions and Nb junctions is that the latter operates above its gap frequency. If we now compare the mixer noise temperature of Nb at 820 GHz (51 K)[6] with NbN at 850 GHz (204 K) it is clear that Nb even above the gap frequency functions much better than a state of the art NbN junction. Further measurements of NbN devices above 1100 GHz need to be performed to examine the feasibility of SIS detection at these frequencies.

We would like to thank N. Whyborn for the adaptation of the two junction tuning design for waveguides. Helpful ideas, discussions and general assistance of H. Bukkems, S. den Hartog, J.B.M. Jegers, J.R. Gao, W. Hulshoff, D. Nguyen, and H.H.A. Schaeffer are acknowledged. This work was supported in part by the European Space Agency under contract No. 7898/88/NL/PB(SC) and the Stichting voor Technische Wetenschappen.

References

[1] H. van de Stadt, A. Baryshev, P. Dieleman, M.W.M. De Graauw, T.M. Klapwijk, S. Kovtonyuk, G. de Lange, I. Lapitskaya, J. Mees, R.A. Panhuyzen, G. Prokopenko, and H.H.A. Schaeffer, *Sixth Int. Symp. on Space THz Techn.*, March 1995, CalTech. Pasadena, California, USA.

[2] M. Bin, M.C. Gaidis, J. Zmuidzinas, T.G. Phillips, and H.G. LeDuc, *Appl. Phys. Lett.*, **68**, pp. 1714-1716 (1996).

[3] Y. Uzawa, Z. Wang, A. Kawakami, *Seventh Int. Symp. on Space THz Techn.*, March 1996, University of Virginia, Charlottesville, Virginia, USA.

[4] A. Karpov, B. Plathner, J. Blondel, M. Schicke, and K.H. Gundlach, *Seventh Int. Symp. on Space THz Techn.*, March 1996, University of Virginia, Charlottesville, Virginia, USA.

[5] G. de Lange, J.J. Kuipers, T.M. Klapwijk, R.A. Panhuyzen, H. van de Stadt, and M.W.M. de Graauw, *J. Appl. Phys.*, **77**, pp. 1795-1804 (1995).

[6] P. Dieleman, T.M. Klapwijk, J.R. Gao, and H. van de Stadt, to be published in *IEEE Trans. Appl. Super.* 1997.

[7] J. Zmuidzinas, H.G. LeDuc, J.A. Stern, and S.R. Cypher, *IEEE Trans Microwave Theory Tech.* **42**, 698-706 (1994).

[8] B.Plathner, M. Schicke, T. Lehnert, K.H. Gundlach, H. Rothermel, M. Aoyagi, and S. Takada, Appl. Phys. Lett. **69**, pp. 4102- 4104 (1996), M. Schicke, K. H. Gundlach, H. Rothermel, P. Dieleman, and H. van de Stadt, unpublished.

[9] C.E. Honingh, J.J. Wezelman, M.M.T.M. Dierichs, G. de Lange, H.H.A. Schaeffer, T.M. Klapwijk, and M.W.M. de Graauw, *J. Appl. Phys.*, **74**, pp. 4762-4773 (1993).

[10] E.L. Wolf, *Principles of Electron Tunneling Spectroscopy*, p 104 (Oxford University Press, New York, 1985).

[11] T.M. Klapwijk, G.E. Blonder, and M. Tinkham, Physica B+C 109 & 110, 1657 (1982), M. Octavio, M. Tinkham, G.E. Blonder, and T.M. Klapwijk, Phys. Rev. B **27**, 6739 (1983).

[12] N. van der Post, E.T. Peters, I.K. Yanson, and J.M. van Ruitenbeek, Phys. Rev. Lett. **73** 2611 (1994).

[13] D. Rogovin and D.J. Scalapino, *Ann. Physics,* **68**, pp.1-90, (1974).

[14] N.B. Dubash, G. Pance, and M.J. Wengler, *IEEE Trans. Microwave Theory Tech.*, **42**, pp 715-725, (1994).

[15] Z. Wang, Y. Uzawa, and A. Kawakami, to be published in *IEEE Trans. Appl. Super.* 1997.

[16] J.A. Stern, H.G. LeDuc, and A.J. Judas, *Third Int. Symp. on Space THz Techn.*, Ann Arbor, MI, USA., (1992).

[17] N.B. Dubash, M.J. Wengler, private communication.

[18] M.J.M. de Jong and C.W.J. Beenakker, Phys. Rev. B **49**, 16070 (1994).

[19] J.R. Tucker, M.J. Feldman, *Rev. Mod. Phys.* **57**, pp. 1055-1113 (1985).

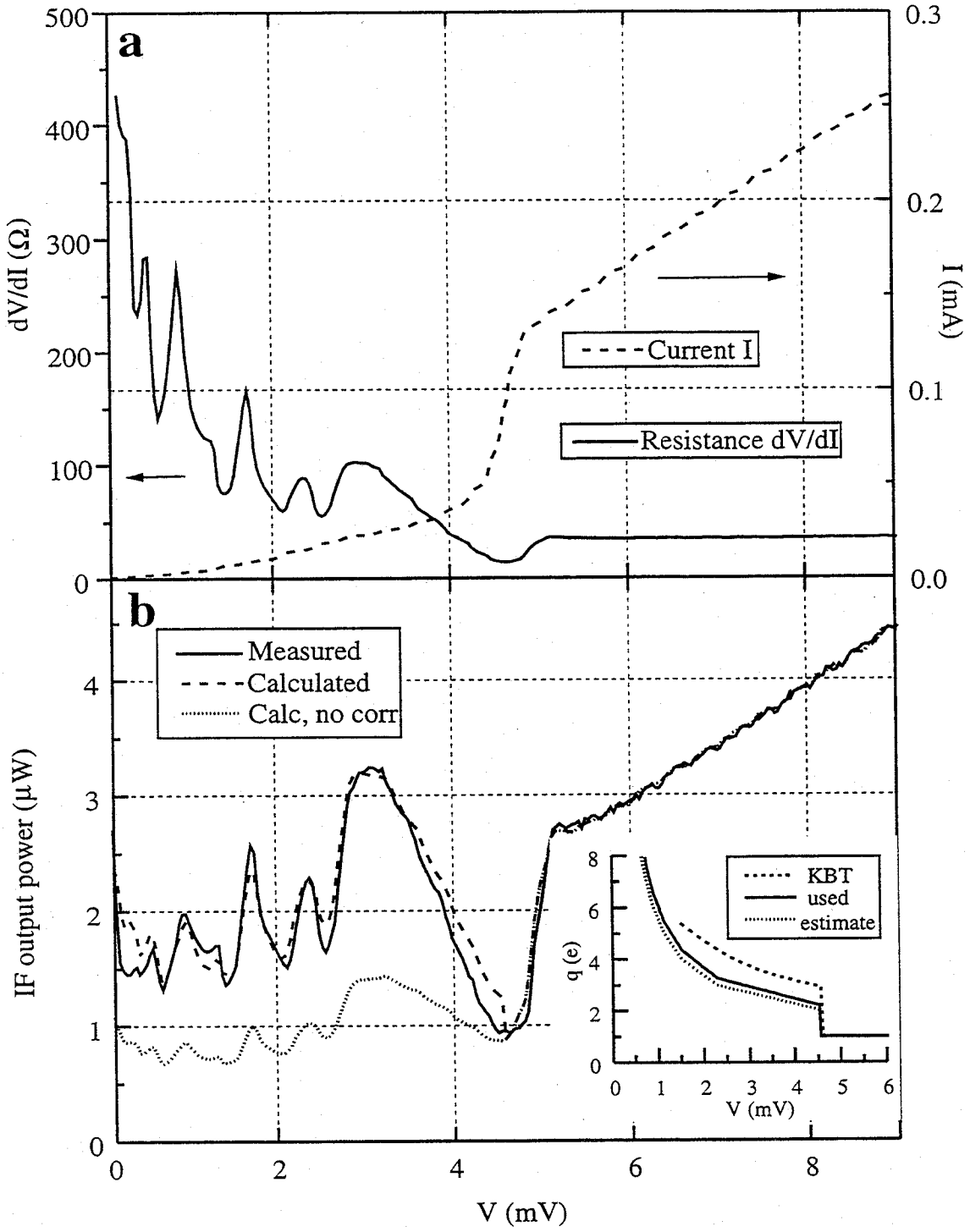

Figure 1: a. I,V and dV/dI characteristics. The dV/dI curve peaks at voltages close to $2\Delta/n$, with $n = 1, 2, 3 \ldots$. b. The output noise power at 1.5 GHz. The dotted curve is calculated using $q = e$, the dashed curve is calculated with the full dependence of q on the voltage as shown by the solid line in the inset. The dashed curve in the inset is calculated as described in the text. Neglecting Andreev reflection above the gap energy results in the dotted curve.

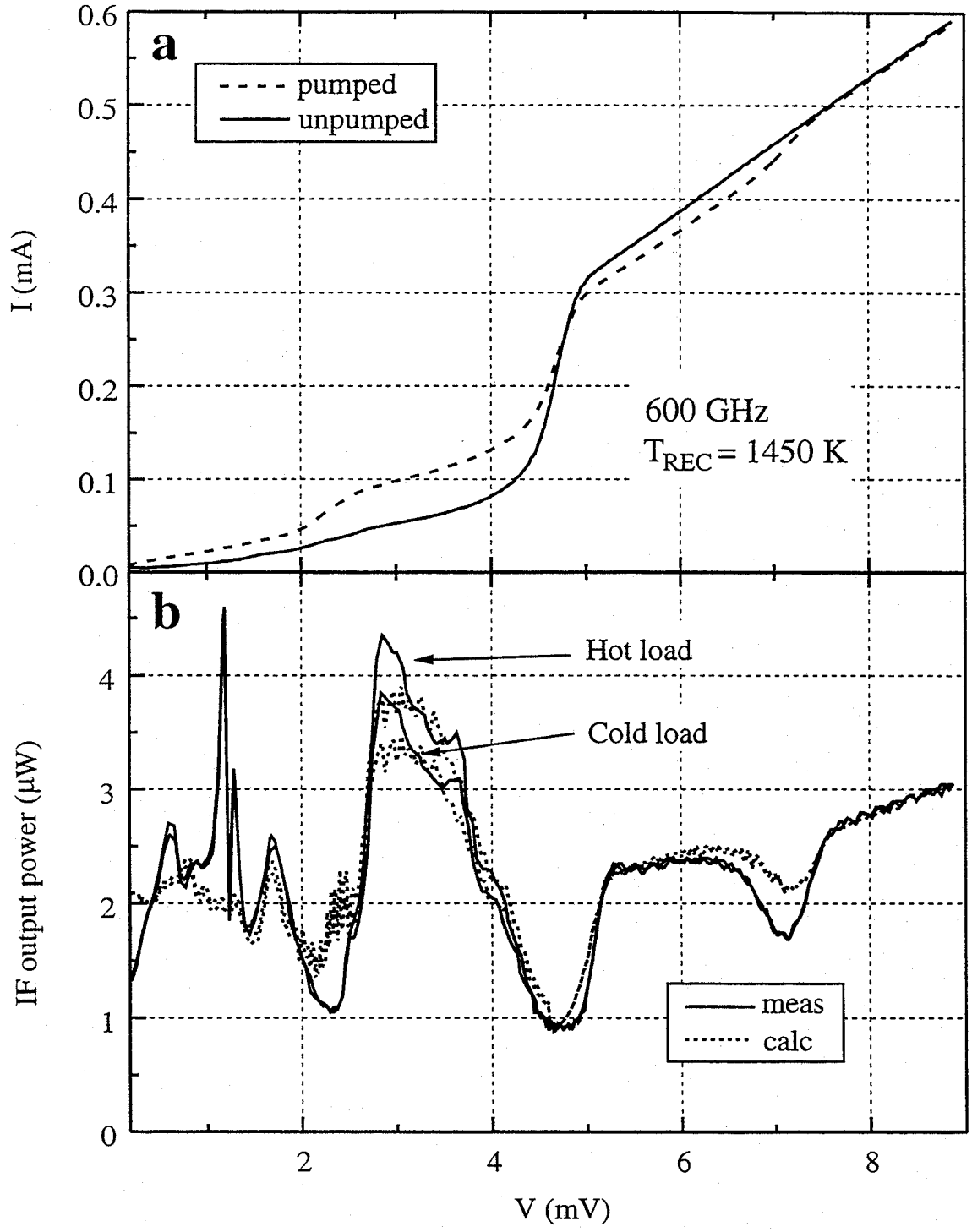

Figure 2: a. Pumped and unpumped I,V curves. The pump frequency is 600 GHz. b. Measured and calculated IF output power for hot and cold loads. The double peak in the measured IF curve at 1.2 mV is due to incomplete suppression of the ac Josephson effect by a magnetic field, possibly because the junctions had unequal areas. Higher order Shapiro steps at multiples of $hf/2e$ =1.24 mV are reasonably well suppressed.